Cellular/Molecular

Group I mGluR Activation Enhances Ca^{2+}-Dependent Nonselective Cation Currents and Rhythmic Bursting in Main Olfactory Bulb External Tufted Cells

Hong-Wei Dong,[1] Abdallah Hayar,[2] Joseph Callaway,[1] Xiang-Hong Yang,[1] Qiang Nai,[1] and Matthew Ennis[1]

[1]Department of Anatomy and Neurobiology, University of Tennessee Health Science Center, Memphis, Tennessee 38163, and [2]Department of Neurobiology and Developmental Sciences, University of Arkansas for Medical Sciences, Little Rock, Arkansas 72205

In the main olfactory bulb, activation of group I metabotropic glutamate receptors (mGluRs) by olfactory nerve stimulation generates slow (2 Hz) oscillations near the basal respiratory frequency. These oscillations arise in the glomerular layer and may be generated, in part, by the intrinsic neurons, the juxtaglomerular neurons. We investigated the physiological effects of group I mGluR agonists on one population of juxtaglomerular neurons, external tufted (ET) cells, which rhythmically burst at respiratory frequencies and synchronize the intraglomerular network. Electrophysiological studies in rat main olfactory bulb slices demonstrated that the mGluR agonist 3,4-dihydroxyphenylglycine (DHPG) amplified the strength of ET cell spike bursts, principally by increasing the number of spikes per burst. Voltage-clamp and Ca^{2+}-imaging studies showed that DHPG elicits a Ca^{2+}-dependent nonselective cation current (I_{CAN}) in the dendrites of ET cells triggered by Ca^{2+} release from internal stores. The DHPG effects on bursting and membrane current were attenuated by flufenamic acid and SKF96365, agents known to antagonize I_{CAN} in a variety of neurons. DHPG also elicited slow membrane current oscillations and spikelets in ET cells when synaptic transmission and intrinsic membrane channels were inoperative. These findings indicate that DHPG may passively (by increasing burst strength) or actively (by increasing conductance of gap junctions) enhance the strength of electrical synapses between ET cells. Together, these findings indicate that activation of group I mGluRs on the dendrites of ET cells play a key role in the generation of slow rhythmic oscillation in the glomerular network, which is in turn tuned to sniffing of the animal *in vivo*.

Introduction

Slow respiratory-driven neural activity is a prominent temporal feature of the rodent main olfactory bulb (MOB) network. Such activity is centered around 1–2 Hz in anesthetized rodents and during noninvestigative sniffing in waking animals (Fontanini and Bower, 2006; Scott, 2006). Spontaneous and olfactory nerve-evoked activity of mitral and tufted cells *in vitro* also occurs at the low end of the theta frequency, suggesting that there are intrinsic mechanisms for respiratory entrainment within the MOB (Buonviso et al., 2006; Scott, 2006). Several studies have demonstrated that activation of group I mGluRs (i.e., mGluR1/5 subtypes) are necessary for slow (1–2 Hz) synchronized oscillatory responses of mitral cells to olfactory nerve stimulation in MOB slices (Schoppa and Westbrook, 2001; Yuan and Knopfel, 2006). The precise location(s) of the mGluRs involved in such oscillations have not been determined. Mitral cells are one obvious candidate due to their robust expression of mGluR1 and findings that mGluR1 activation enhances mitral cell excitability (Masu et al., 1991; Martin et al., 1992; Shigemoto et al., 1992; van den Pol, 1995; Heinbockel et al., 2004; Ennis et al., 2006; De Saint Jan and Westbrook, 2007).

External tufted (ET) cells located within the glomerular layer may also play a key role in mGluR-dependent synchronous slow oscillatory activity in the MOB. ET cells rhythmically burst at theta frequencies *in vitro* and play a major role in synchronizing the glomerular network (Hayar et al., 2004a,b, 2005). Like mitral cells, ET cells appear to express mGluR1 and may also express the mGluR5 subtype (Shigemoto et al., 1992; Romano et al., 1995; Sahara et al., 2001; Heinbockel et al., 2004). The functional role of group I mGluRs in regulating the activity of ET neurons is unknown. The goal of the present study, therefore, was to investigate the actions of group I mGluR activation and inactivation on the activity of ET cells using patch-clamp electrophysiology.

We found that group I mGluR agonists robustly increase the strength of rhythmic ET cell spike bursts. This enhancement is at least partially due to activation of a depolarizing Ca^{2+}-dependent nonselective cation current in ET cell dendrites. When synaptic transmission is blocked in the slice, mGluR agonists elicit slow rhythmic membrane current oscillations in ET cells that appear to be mediated by electrical synapses between these cells. These findings demonstrate that activation of group I mGluRs on ET cells in the glomerular layer play a key role in the generation of slow oscillations in the MOB network.

Received Jan. 13, 2009; revised June 24, 2009; accepted Aug. 16, 2009.

This work was supported by National Institutes of Health Grants DC09049, DC06356, DC07123, RR020146, DC03195, and DC08702.

Correspondence should be addressed to Hong-Wei Dong, Department of Anatomy and Neurobiology, University of Tennessee Health Science Center, 855 Monroe Avenue, Suite 515, Memphis, TN 38163. E-mail: hdong5@utmem.edu.

DOI:10.1523/JNEUROSCI.0206-09.2009

 0270-6474/09/2911943-11$15.00/0

Materials and Methods

Sprague Dawley rats (15–25 d old, of either sex) were decapitated in accordance with Institutional Animal Care and Use Committee and National Institutes of Health guidelines. The olfactory bulbs were removed and immersed in oxygenated sucrose–artificial CSF (ACSF) composed of the following (in mM): 26 $NaHCO_3$, 1.25 NaH_2PO_4, 3 KCl, 4 $MgSO_4$, 0.1 $CaCl_2$, 20 glucose, and 234 sucrose; pH 7.3, 310 mOsm. Horizontal slices were cut with a Vibratome 3000 (Vibratome) at thickness of 400 μm. After recovery at 30°C for 15 min, slices were then incubated until used at room temperature (22°C) in normal ACSF equilibrated with carbogen (95% O_2–5% CO_2) and composed of the following (in mM): 126 NaCl, 26 $NaHCO_3$, 3 KCl, 1.25 NaH_2PO_4, 2 $MgCl_2$, 2 $CaCl_2$, and 20 glucose (pH 7.3, 310 mOsm). For experiments containing cadmium and nickel in the ACSF, NaH_2PO_4 was excluded. For recording, a single slice was placed in a recording chamber and continuously perfused with carbogen-saturated ACSF at the rate of 1.5 ml/min.

Electrophysiology. All recordings were performed at 30°C. Neurons were visualized using an upright microscope (BX50WI; Olympus Optical) equipped with epifluorescence and near-infrared differential interference contrast (DIC) optics. Whole-cell current and voltage-clamp recordings were made with Axopatch 200B and MultiClamp 700B amplifiers (Molecular Devices). The pipette resistance was 11–13 MΩ. The junction potential was 9–10 mV, and all reported voltage measurements were uncorrected for these potentials. Only neurons with access resistance <30 MΩ were included in this study. Unless otherwise noted, voltage-clamp recordings from ET cells were made with pipettes containing (in mM): 125 cesium methanesulfonate ($CsMeSO_3$), 1 NaCl, 10 phosphocreatine ditris salt, 3 MgATP, 0.3 Na_2GTP, 0.5 EGTA, 10 HEPES, and 10 QX-314 (pH 7.3, 290 mOsm). The intracellular solution for current-clamp recording was composed of the following (mM): 124 potassium gluconate, 1 NaCl, 10 phosphocreatine ditris salt, 3 MgATP, 0.3 Na_2GTP, 0.5 EGTA, and 10 HEPES; pH 7.3, 290 mOsm. Lucifer yellow (0.02%) and biocytin (0.2%, Molecular Probes) were added to the intracellular solution in all experiments for *in situ* and *post hoc* labeling, respectively. Extracellular spikes were recorded with ACSF-filled patch pipettes as action currents in cell-attached voltage-clamp mode.

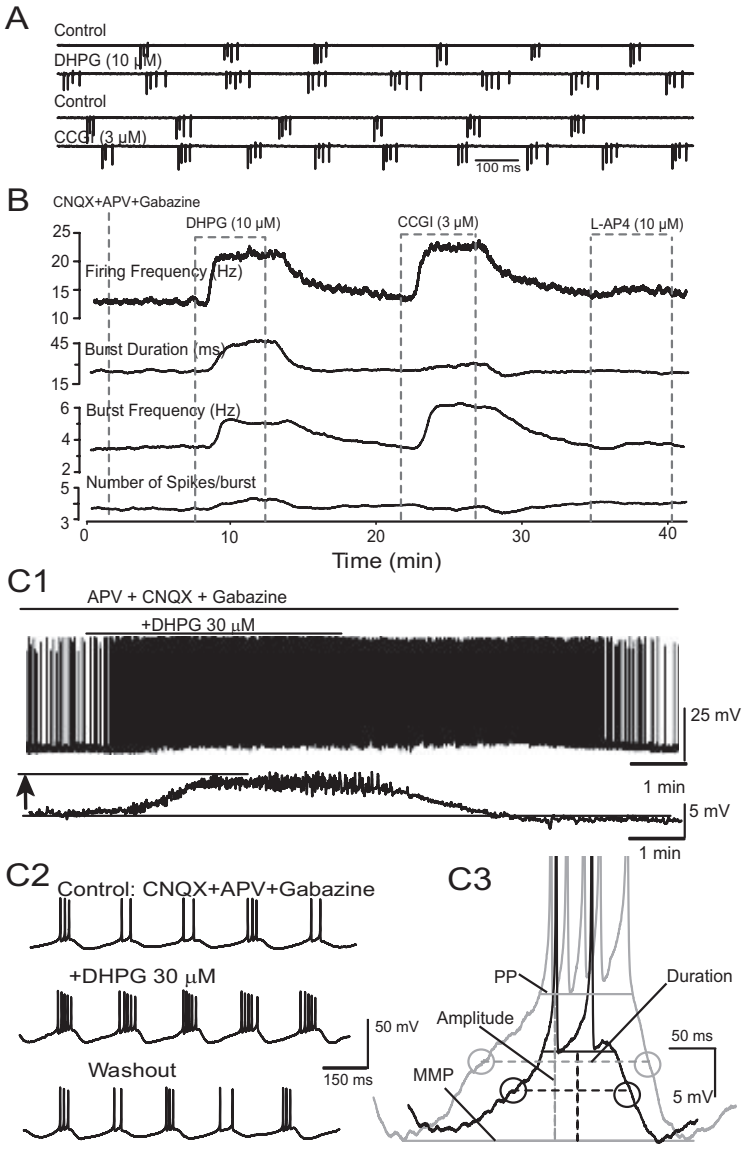

Figure 1. DHPG increases the strength of ET cell bursting. ***A***, Sample extracellular recordings (cell-attached, voltage-clamp mode) from an ET cell show that bath-applied DHPG (10 μM) and L-CGG-I (3 μM), but not L-AP4, increase properties of rhythmic spike bursts; all experiments in this figure were performed with ACSF containing CNQX-APV-gabazine. ***B***, Running average showing the effects of DHPG, CCGI, and L-AP4 on bursting parameters. ***C1***, Whole-cell current-clamp trace showing that DHPG (30 μM) depolarized and increased the discharge of this ET cell; the depolarization is more clearly seen in the lower filtered (0.5 Hz) trace. ***C2***, Faster timescale records for the cell shown in ***C1***. Note increase in the number of spikes per burst. ***C3***, DHPG increased the amplitude and duration of the slow depolarizing envelope underlying ET cell spike bursts; same cell as in ***C1*** and ***C2***. Dashed horizontal lines denote AMP; PP, peak potential (see Materials and Methods for details).

Analog signals were low-pass filtered at 2 kHz and digitized at 5 kHz using a Digidata-1322A interface and pClamp 9 software (Molecular Devices). *I–V* relationships of evoked currents were studied with a voltage ramp protocol (−80 mV to +30 mV, 70 mV/s, 1.5 s duration) from a holding potential (HP) of −60 mV; membrane resistance was calculated from currents elicited by negative voltage pulses (−20 mV, 200 ms duration). Effects of mGluR agonists on ET cell membrane potential, burst duration and amplitude were calculated from current-clamp records (20 s epochs; low-pass filtered at 0.5 Hz) (see Fig. 1*C*). The resting potential or minimum membrane potential (MMP) was defined as the nadir of the membrane potential during the interburst interval (Liu and Shipley, 2008). The peak potential was defined as the membrane potential from which the first spike in the burst was launched. The average membrane potential (AMP) of the burst was calculated as the average of the MMP and the peak potential. The duration of depolarizing envelope of the spike burst was calculated as the interval between the AMP point on the rising and falling phases of the slow depolarizing envelope (see Fig. 1*C3*). Membrane current autocorrelograms were constructed from 5–10 s recording samples in each experimental condition. Membrane current traces were offset by their mean, and the traces were then reduced by group averaging to one point per 5 ms. Autocorrelograms of the conditioned traces were constructed and normalized by the autocorrelation coefficient of the traces at zero lag time. The coefficients of correlation (theoretical maximum = 1) measure the rhythmicity of membrane current oscillations, also evident by regularly occurring sidebands in the autocorrelogram.

Spike detection was performed off-line using the Minianalysis program (Synaptosoft). Custom-designed computer algorithms were used

off-line to evaluate the following parameters of ET cell spike bursts: overall firing frequency, bursting frequency (defined as the number of bursts per second), spikes per burst, and burst duration (defined as the time interval between the first and the last spike in a burst). A burst of spikes was defined as a series of two or more consecutive spikes that had interspike time intervals of <75 ms as previously reported (Hayar et al., 2004a).

ET cells were identified by their characteristic electrophysiological and morphological characteristics (Hayar et al., 2004a,b, 2005; Hayar and Ennis, 2007; Liu and Shipley, 2008). Electrophysiologically, they exhibited spontaneous rhythmic bursting in cell-attached (see Figs. 1*A*, 2*A1*) or current-clamp (see Figs. 1*C*, 7*A*) recordings. Rhythmic bursting was typically confirmed in extracellular recordings before switching to whole-cell voltage-clamp mode. Cells lacking rhythmic bursting were not studied. Additionally, ET cells exhibit randomly occurring spontaneous EPSCs in voltage-clamp recordings (HP = −60 mV) (see Fig. 2*A2*), whereas periglomerular and short axon cells exhibit EPSCs clustered in bursts (Hayar et al., 2004a,b, 2005). Morphologically, all 62 rhythmically bursting ET cells filled intracellularly with Lucifer yellow and/or biocytin were characterized by a pear-shaped soma within the glomerular layer and an apical dendrite with a tuft-like arborization that ramified within a single glomerulus (see Fig. 2*A3*); there was no evidence of secondary dendrites that extended into the external plexiform layer in these cells. Similar morphological characteristics were observed for 17 cells filled with fura-2 that were initially identified as ET cells based on spontaneous EPSC pattern in voltage-clamp recordings (see Figs. 4*A1*,*B1*, 5*A*,*C*).

Calcium imaging. Optical imaging of calcium signals was combined with electrophysiology in some experiments. For these studies, the patch pipette (5–7 MΩ) contained the calcium-sensitive indicator fura-2 pentapotassium salt (100 μM) and the following (in mM): 120 $CsMeSO_3$, 10 phosphocreatine, 10 HEPES 1 Na_2ATP, 1 MgATP, 0.3 Na_2 GTP, and 10 QX-314; 280 mOsm, pH 7.3. fura-2 was excited at a wavelength of 380 ± 10 nm and fluorescence changes were measured at an emission wavelength of 520 ± 40 nm (filters from Chroma Technology). Electrical and optical data were synchronously acquired on single Windows platform PC running software written by J. C. Callaway, based on software developed by Lasser-Ross et al. (1991). Electrical signals were acquired using a AxoPatch 200B amplifier (Molecular Devices) and digitized with 16 bit resolution at 10 kHz. Optical recordings were obtained using a Till Photonics Sensicam cooled CCD camera at a frame rate of 50 Hz. $\Delta F/F$ is the ratio of the change in fluorescence at 380 nm (ΔF) divided by the fluorescence (F) measured immediately after opening the shutter. The percentage change of ($\Delta F/F$) was used for statistical analysis. Fluorescence measurements were corrected for bleaching by subtracting the decrease in fluorescence that occurred when the cell was held at −60 mV without stimulation. Autofluorescence correction was performed by subtracting the fluorescence of a nearby region of the slice with no fura-2 fluorescence from the measured initial value of F.

Electrophysiological and calcium imaging data, expressed as mean ± SEM, were statistically analyzed using one-way ANOVA followed by *post hoc* comparisons (Newman–Keuls tests), or with Student's t tests.

Drugs and solutions. Low-Na^{2+} ACSF was prepared by replacing NaCl with an equimolar concentration of sucrose. Nominally Ca^{2+}-free ACSF was prepared by replacing 2 mM Ca^{2+} with an equimolar concentration of Mg^{2+}. In most experiments, drugs and solutions were applied to the perfusion solution with a three-way valve system. In some experiments, 3,4-dihydroxyphenylglycine (DHPG, 1 mM) was focally applied by pressure application (100 ms duration, 20 psi) from patch pipettes (~2 μm tip diameter) using a picospritzer (General Valve). Recording medium, pipette solution, 5-*N*-(2,6-dimethylphenylcarbamoylmethyl)triethylammonium bromide (QX-314), gabazine (SR 95531), 6-cyano-7-nitroquinoxaline-2,3-dione (CNQX), (±)-2-amino-5-phosphopentanoic acid (APV), cadmium chloride, nickel (II) chloride hexahydrate, flufenamic acid (FFA), and 1,2-bis(2-amino-phenoxy)ethane-*N*,*N*,*N*′,*N*′-tetraacetic acid (BAPTA), were obtained from Sigma-Aldrich. DHPG, L-CCG-I, LY367385, 2-methyl-6-(phenylethynyl)-pyridine (MPEP), SKF96365, tetrodotoxin (TTX), and thapsigargin were purchased from Tocris Bioscience.

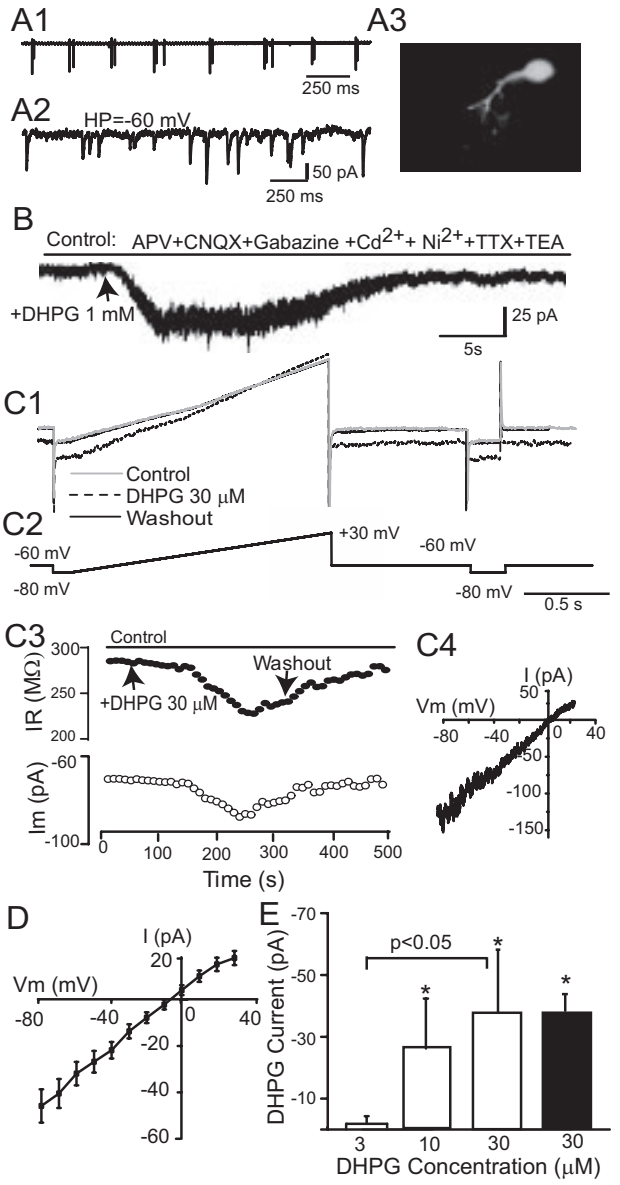

Figure 2. DHPG evokes an inward current in ET cells. ***A***, An ET cell recorded in whole-cell voltage-clamp mode was initially identified on the basis of extracellularly recorded spike bursts (***A1***). In voltage-clamp mode, sEPSCs occurred randomly (***A2***). ***A3***, Lucifer yellow staining shows the morphology of this typical ET cell. ***B***, A focal puff of DHPG (1 mM) adjacent to this ET cell evoked an inward current at a HP of −60 mV. ***C1***, ***C2***, Membrane currents (***C1***) produced by slow voltage ramps (***C2***, command voltages) were used to generate *I–V* curves before and during bath-applied DHPG (30 μM), and again after washout; at right, hyperpolarizing pulses monitored changes in input resistance. ***C3***, The inward current elicited by bath-applied DHPG is accompanied by decreased membrane resistance (HP = −60 mV). ***C4***, The DHPG-evoked current for a single ET cell, obtained by subtraction of the control and DHPG *I–V* curves in ***C1***, was linear and reversed polarity near 0 mV. ***D***, Mean *I–V* plot of the DHPG current in 27 ET cells; the mean reversal potential was −5.2 ± 2.3 mV. ***E***, Dose–response relationship of DHPG-evoked currents in ET cells. The magnitude of the inward current elicited by cumulative doses of 3, 10, and 30 μM DHPG were measured in individual ET cells (open bars, $n = 6$, HP = −60 mV); 10 and 30 μM DHPG significantly increased the amplitude of the inward current relative to baseline (*$p < 0.05$ one-way repeated-measures ANOVA followed by Newman–Keuls tests), and the currents evoked by 30 μM were significantly greater than that evoked by 3 μM ($p < 0.05$, Newman–Keuls test). The amplitude of the inward current elicited by a single 30 μM application of DHPG (black bar, $n = 27$) did not differ from that elicited in the cumulative condition ($p > 0.05$, unpaired t test).

Results

mGluR activation enhances ET cell rhythmic bursting

We first examined the effect of the selective group I mGluR agonist DHPG on ET cell spontaneous bursting using extracellular recordings. DHPG was applied in the presence of antagonists of ionotropic glutamate and GABA receptors (CNQX 10 μM, APV 50 μM, and gabazine 10 μM) to minimize network interactions. In all cases ($n = 7$ cells), bath application of DHPG (10–30 μM) robustly and reversibly increased the strength of ET cell bursting (Fig. 1*A*,*B*). DHPG significantly increased the bursting frequency from 2.7 ± 0.4 bursts/s to 3.7 ± 0.4 bursts/s ($p < 0.01$, paired *t* test) and the number of spikes per burst from 4.4 ± 0.7 spikes per burst to 5.3 ± 0.7 spikes per burst ($p < 0.05$, paired *t* test). Together, the increase in bursting frequency and number of spikes per burst raised the mean firing frequency from 10.8 ± 0.7 spikes/s to 20.3 ± 3.7 spikes/s ($p < 0.05$, paired *t* test). The duration of the spike burst increased from 36 ± 4 ms to 49 ± 10 ms ($p < 0.05$, paired *t* test). Similar effects of DHPG were observed in normal ACSF lacking CNQX-APV-gabazine (supplemental Fig. 1*A*, available at www.jneurosci.org as supplemental material). We also examined the effects of preferential group II and III mGluR agonists in a subset of ET cells in the presence of CNQX-APV-gabazine (Fig. 1*A*). The group II agonist L-CCG-I (3 μM, $n = 7$) increased the burst frequency (2.9 ± 0.5 Hz vs 3.8 ± 0.6 Hz, $p < 0.05$ paired *t* test), the number of spikes per burst (4.0 ± 0.4 vs 4.8 ± 0.4, $p < 0.05$, paired *t* test), mean firing frequency (10.9 ± 1.1 Hz vs 17.5 ± 2.3 Hz, $p < 0.01$, paired *t* test), and the burst duration (32.1 ± 4.6 ms vs 40 ± 6.6 ms, $p < 0.05$, paired *t* test). In contrast, the group III mGluR agonist AP4 (10 μM, $n = 3$) had no discernible effect on the properties of ET cell bursting (burst frequency: 3.8 ± 0.4 Hz vs 4.0 ± 0.4 Hz, $p > 0.05$; number of spike/burst: 3.5 ± 0.4 vs 3.4 ± 0.4, $p > 0.05$, paired *t* tests). These findings suggest that both group I and II mGluRs directly enhance ET excitability and rhythmic bursting. The actions of group II mGluRs were not pursued further in the present study.

In whole-cell current-clamp mode, DHPG (30 μM) reversibly increased the parameters of bursting measured in the extracellular recordings above (Fig. 1*C*; see also Fig. 7). DHPG induced a depolarization of 7.3 ± 1.1 mV ($n = 11$), a value similar to that that predicted (7.4 mV) from the inward current produced by DHPG (37.7 pA, see below) and the average ET cell input resistance (196 ± 12 MΩ) (Fig. 1*C1*). DHPG also increased the amplitude (8.4 ± 0.8 mV to 11.1 ± 1.5 mV, $p < 0.01$, paired *t* test, $n = 10$) (Fig. 1*C3*) and duration (174 ± 14 ms to 237 ± 20 ms, $p < 0.01$, paired *t* test, $n = 10$) of the depolarizing envelope. The DHPG-evoked increase in the number of spikes per burst was significantly and positively correlated with the basal number of spikes per burst ($R^2 = 0.43$, $p < 0.05$); it was not correlated with the degree of DHPG-evoked depolarization or the resting membrane potential.

Group I mGluRs include mGluR1 and mGluR5. Both subtypes are expressed by neurons in the glomerular layer although the specific cell type(s) have not been definitively identified (Shigemoto et al., 1992; Fotuhi et al., 1993; Romano et al., 1995; van den Pol., 1995; Sahara et al., 2001; Heinbockel et al., 2004). The enhancement of bursting was prevented when DHPG (30 μM) was applied in presence of the mGluR1 and mGluR5 antagonists LY367385 (100 μM) and MPEP (50 μM), respectively (supplemental Fig. 1*B*, available at www.jneurosci.org as supplemental material). We also observed that LY367385 and MPEP significantly reduced olfactory nerve-evoked EPSCs elicited in normal ACSF, indicating that endogenously released glutamate can activate mGluRs on ET cells (supplemental Fig. 1*C*, available at www.jneurosci.org as supplemental material).

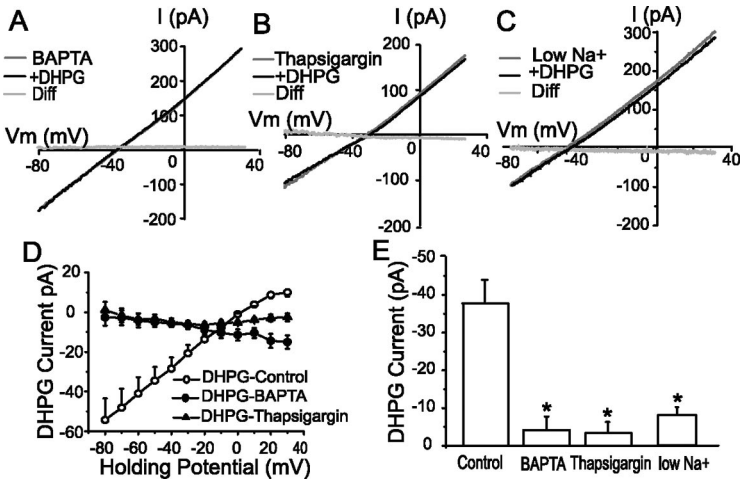

Figure 3. I_{DHPG} requires intracellular Ca^{2+} and is largely mediated by Na^+ influx. ***A***, *I–V* curves generated from recordings with a BAPTA-based internal solution (BAPTA, see text) before and during application of DHPG (30 μM, +DHPG); the subtraction *I–V* curve (Diff) shows that DHPG-evoked currents were nil with BAPTA. ***B***, *I–V* curves generated from recordings with the standard pipette solution in the presence of the Ca^{2+} store-depleting agent thapsigargin (1 μM) before and during application of DHPG; the subtraction *I–V* curve (Diff) shows that DHPG did not evoke an appreciable current in the presence of thapsigargin. ***C***, *I–V* curves generated in the presence of low-Na^+ ACSF (reduction from 152 to 51 mM) before and after bath application of DHPG (30 μM); the subtraction *I–V* curve (Diff) shows that DHPG did not evoke an appreciable current in low-Na^+ ACSF. ***D***, Group data subtraction *I–V* curves showing the effect of DHPG (30 μM) in control, BAPTA, and thapsigargin conditions. ***E***, Group data illustrating the magnitude of I_{DHPG} (HP = −60 mV) in the above three conditions. Note that BAPTA ($n = 6$), thapsigargin ($n = 4$), and low Na^+ ($n = 8$) replacement significantly and nearly completely abolished I_{DHPG}; $^*p < 0.05$ compared with control ($n = 27$), unpaired *t* tests.

DHPG activates a nonselective cation current in ET cells

Voltage-clamp recordings were used to investigate currents elicited by DHPG. Preliminary studies (Dong et al., 2007) indicated that a major portion of DHPG-evoked inward currents persisted following blockade of ionotropic glutamate and GABA receptors, and fast Na^+ and voltage-gated Ca^{2+} channels (VGCCs). Therefore, the following experiments were conducted in a modified ACSF containing CNQX-APV-gabazine, 1 μM TTX, 200 μM cadmium (Cd), 1 mM nickel (Ni), and 10 mM TEA unless otherwise noted. Separate experiments showed that these concentrations of Cd and Ni completely blocked Ca^{2+} currents and transients in ET cells evoked by intracellular depolarization (see supplemental Fig. 2, available at www.jneurosci.org as supplemental material). Under these conditions, bath or puff application of DHPG elicited an inward current (I_{DHPG}) in ET cells (Fig. 2*B*,*C*). I_{DHPG} was accompanied by a reduction in input resistance (Fig. 2*C3*); bath-applied DHPG (30 μM) decreased the input resistance by 56.0 ± 9.9 MΩ. The *I–V* relation of I_{DHPG} obtained by subtracting the current recorded in the presence the absence of DHPG was relatively linear across the range of membrane potentials examined (−80 to +30 mV) (Fig. 2*C4*). The mean reversal potential of I_{DHPG} was −5.2 ± 2.3 mV (range −27.3 to 19 mV, $n = 27$) (Fig.

2*D*). The amplitude of I_{DHPG} increased in a concentration-dependent manner with bath application of 3, 10, and 30 μM DHPG (Fig. 2*E*) ($n = 6$).

Repetitive puff or bath application of DHPG at 4–6 min intervals with an intervening washout produced comparable responses that did not significantly differ (supplemental Fig. 3, available at www.jneurosci.org as supplemental material). Thus, responses to DHPG in individual ET cells were consistent and stable, providing an important control for the multiple DHPG application experiments below. LY367385 (100 μM) or MPEP (50 μM) significantly and reversibly reduced, but did not completely block, I_{DHPG} (supplemental Fig. 4*A1*,*A2*,*B*, available at www.jneurosci.org as supplemental material). LY367385 reduced I_{DHPG} by 59.2 ± 11.8% and MPEP by 68.1 ± 11.3% (supplemental Fig. 4*C*, available at www.jneurosci.org as supplemental material) ($p < 0.01$, paired *t* tests). Combined application of LY367385 and MPEP blocked I_{DHPG} (93.6 ± 13.2% reduction) (supplemental Fig. 4*A3*,*B*,*C*, available at www.jneurosci.org as supplemental material). These results suggest that I_{DHPG} in ET cells is mediated by both mGluR1 and mGluR5. Together, the preceding findings demonstrate that DHPG evokes a robust inward current at or near the resting membrane potential of ET cells. The properties of this current (increased conductance, reversal potential near 0 mV) suggest that activation of group I mGluRs activates a nonselective cation current in ET cells as in variety of neurons (Anwyl, 1999). The conductance increase associated with I_{DHPG} suggests that it is not mediated by activation of an electrogenic Na^+–Ca^{2+} exchanger as has been observed for some mGluR-mediated currents (Staub et al., 1992; Keele et al., 1997; Lee and Boden, 1997; Anwyl, 1999).

I_{DHPG} requires internal Ca^{2+}

mGluR-activated nonselective cation currents may be Ca^{2+} dependent (I_{CAN}), activated secondarily to a rise in intracellular Ca^{2+}, or Ca^{2+} independent (Anwyl, 1999). The Ca^{2+} necessary to activate DHPG-evoked I_{CAN} may derive from transmembrane flux or release from intracellular stores (Llano et al., 1991; Yuzaki and Mikoshiba, 1992; Finch and Augustine, 1998; Takechi et al., 1998; Anwyl, 1999). To determine whether intracellular Ca^{2+} is necessary for I_{DHPG}, we first compared currents recorded with standard internal solution to those obtained with an internal solution containing the Ca^{2+} chelator BAPTA (10 mM) to clamp intracellular Ca^{2+} to negligible levels. Inclusion of BAPTA virtually abolished I_{DHPG} at all membrane potentials (Fig. 3*A*,*D*,*E*). At −60 mV, the magnitude of I_{DHPG} (30 μM) recorded with the BAPTA internal solution (−4.1 ± 3.5 pA, $n = 6$) was significantly smaller than with the standard internal solution (−37.7 ± 5.1, $n = 27$, $p < 0.01$, unpaired *t* test (Fig. 3*E*). To investigate the role of extracellular Ca^{2+} we compared the magnitude of I_{DHPG} in modified ACSF (i.e., containing CNQX-APV-gabazine-TTX-Cd-Ni-TEA) to that in nominally Ca^{2+}-free modified ACSF. In Ca^{2+}-free modified ACSF, DHPG (30 μM) evoked an inward current of −26.5 ± 4.5 pA (HP = −60 mV, $n = 5$; data not shown) that was not significantly different from that in modified ACSF ($p > 0.05$, unpaired *t* test). The preceding findings demonstrate that I_{DHPG} is abolished by intracellular Ca^{2+} chelation but persists when extracellular Ca^{2+} is eliminated or with the modified ACSF that abolished VGCC-mediated currents in ET cells (supplemental Fig. 2, available at www.jneurosci.org as supplemental material). Therefore, I_{DHPG} does not appear to depend on transmembrane Ca^{2+} influx via VGCCs or the I_{CAN} channels themselves. Together, these results suggest that I_{DHPG} is an I_{CAN} that depends on a rise in intracellular Ca^{2+} that derives from release from internal stores.

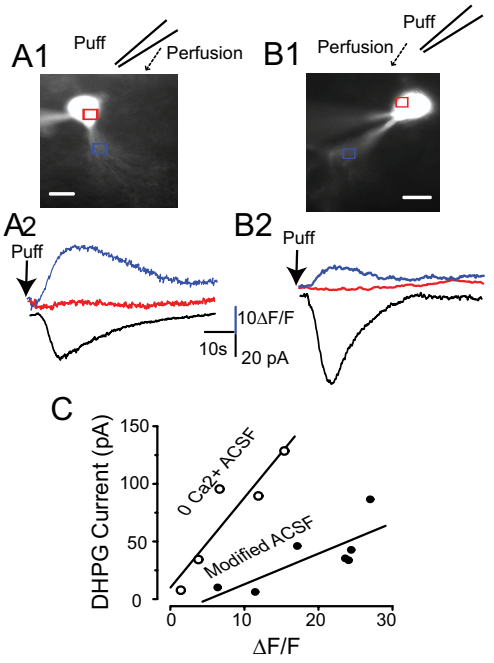

Figure 4. I_{DHPG} is associated with a rise in $[Ca^{2+}]_i$. ***A1***, Fluorescence image of an ET cell recorded with a pipette containing 100 μM fura-2 and voltage clamped at −60 mV; the position of the puffer pipette is shown and the arrow denotes flow of ACSF. ***A2***, $[Ca^{2+}]_i$ transients in the soma and dendrites (red and blue traces respectively, from the regions indicated by rectangles in ***A1***), and current (black trace) evoked by a DHPG puff (1 mM) 30 μm upstream from the soma. Experiments in ***A*** conducted with modified ACSF containing APV-CNQX-gabazine-TTX-TEA-Cd-Ni. ***B1***, ***B2***, The protocol is identical to ***A1*** and ***A2*** above except that Ca^{2+}-free ACSF (no antagonists or channel blockers) was used. Scale bars: ***A1***, ***B1***, 10 μm. ***C***, The magnitude of I_{DHPG} was linearly related to the rise in dendritic $[Ca^{2+}]_i$ in modified ACSF ($R^2 = 0.60$, $p < 0.05$, $n = 7$) or Ca^{2+}-free ACSF ($R^2 = 0.84$, $p < 0.05$, $n = 5$).

To directly investigate the role of Ca^{2+} release from internal stores, we tested the effects of thapsigargin (1 μM), a Ca^{2+} store-depleting agent that blocks the endoplasmic Ca^{2+}-ATPase and thus depletes both inositol triphosphate and ryanodine receptor-sensitive stores (Sagara et al., 1992). As shown in Figure 3, *B* and *D*, the effect of bath-applied thapsigargin was similar to that of BAPTA—I_{DHPG} was completely blocked at all membrane potentials ($n = 4$). For example, the magnitude of the I_{DHPG} at −60 mV was significantly reduced (−3.6 ± 2.7 pA vs modified ACSF; $p < 0.05$, unpaired *t* test) (Fig. 3*E*).

I_{DHPG} is largely mediated by Na^+ influx

Na^+ ions are typically the major inward charge carrier of mGluR-activated nonselective cation currents (Crépel et al., 1994; Anwyl, 1999; Tempia et al., 2001; Tozzi et al., 2003; Berg et al., 2007). To investigate the role of Na^+ ions in I_{DHPG}, we decreased extracellular Na^+ in modified ACSF from 152 mM to 51 mM (see Materials and Methods). As shown in Figure 3, *C* and *E*, reducing extracellular Na^+ attenuated I_{DHPG} at all membrane potentials. The amplitude of I_{DHPG} measured at −60 mV (−8.2 ± 1.6 pA, $n = 8$) with 51 mM extracellular Na^+ was significantly reduced compared with 152 mM Na^+ ($p < 0.001$, unpaired *t* test).

I_{DHPG} is accompanied by a simultaneous rise in dendritic $[Ca^{2+}]_i$

The results to this point lead us to hypothesize that DHPG elicits an I_{CAN} in ET cells dependent on release of Ca^{2+} from internal

stores. To directly test this hypothesis, we monitored intracellular Ca^{2+} ($[Ca^{2+}]_i$) levels and membrane current during application of DHPG. Individual ET cells were loaded with the fluorescent Ca^{2+} indicator fura-2 (100 μM) and membrane currents were measured at −60 mV. The inward current evoked by DHPG puffs did not significantly differ when recorded with fura-2 (−37.7 ± 10.1 pA) or standard internal solutions (−30.7 ± 8.9 pA) (supplemental Fig. 3, available at www.jneurosci.org as supplemental material) ($p > 0.05$, unpaired t test). As shown in Figure 4*A*, in modified ACSF identical to that used to measure I_{DHPG} above (CNQX-APV-gabazine-TTX-Cd-Ni-TEA), a focal puff of DHPG (1 mM) 30–40 μm away from ET cells elicited a simultaneous rise in dendritic ($[Ca^{2+}]_i$ and an inward current. The peak increase in $[Ca^{2+}]_i$ ($\Delta F/F$, 19.2 ± 2.9) was strongly and positively correlated with the magnitude of I_{DHPG} (−37.7 ± 10.1 pA, $R^2 = 0.6$, $p < 0.05$, $n = 7$, regression analysis) (Fig. 4*C*). Bath application of thapsigargin (1 μM) eliminated the inward current (−1.1 ± 0.7 pA) and the rise in $[Ca^{2+}]_i$ ($\Delta F/F$: 0.4 ± 0.2) elicited by DHPG puffs ($n = 3$; data not shown).

Although VGCCs were blocked in the preceding experiment, it is possible that Ca^{2+} may enter the cell via the I_{CAN} channels themselves. To examine the potential role of transmembrane Ca^{2+} influx via I_{CAN} channels, we investigated the effects of DHPG in nominally Ca^{2+}-free ACSF; ionotropic glutamate and GABA receptor antagonists, as well as voltage-gated channel blockers were omitted. DHPG (1 mM) puffs in Ca^{2+}-free ACSF elicited a robust inward current that was positively correlated with the peak increase in $[Ca^{2+}]_i$ (71.1 ± 21.9 pA, $\Delta F/F$ = 7.8 ± 2.6, $R^2 = 0.84$, $p < 0.05$, $n = 5$) (Fig. 4*B*,*C*). The finding that the magnitude of I_{DHPG} in modified and Ca^{2+}-free ACSF is linearly related to the rise in $[Ca^{2+}]_i$ provides further evidence that I_{DHPG} is an I_{CAN} that is triggered by intracellular Ca^{2+} deriving largely from release from internal stores. The peak rise in $[Ca^{2+}]_i$ in Ca^{2+}-free ACSF was significantly lower than that in modified ACSF ($p < 0.05$, unpaired t test), but the magnitude of I_{DHPG} did not significantly differ in the two conditions ($p > 0.05$, unpaired t test). The smaller increases in $[Ca^{2+}]_i$ in Ca^{2+}-free ACSF may be due to lower baseline intracellular Ca^{2+} levels and/or partial depletion from internal stores (Carlson et al., 1997).

We observed that DHPG puffs near the ET cell soma produced increases in $[Ca^{2+}]_i$ that occurred first in the dendrites. To compare the response latency in different cellular compartments, linear fits of the rising phase of the fluorescence curve from six randomly selected ET cells (Fig. 5*C*) were plotted and the x-axis (time) intercepts were taken as the initial latency value. As shown in the Figure 5, regardless of the location of the soma and dendrites with respect to the puffer pipette, the $[Ca^{2+}]_i$ transient was first observed in the distal dendrites. The distal dendritic response, 3.0 ± 0.2 s, was significantly shorter than that in the soma, 4.1 ± 0.4 s ($p < 0.001$, ANOVA followed by Newman–Keuls test). The distal dendritic response latency did not differ from that in the proximal dendrites (3.2 ± 0.3 s, $p > 0.05$) (Fig. 5*D*). The peak rise in $[Ca^{2+}]_i$ in the distal dendrites ($\Delta F/F$: 25.2 ± 3.3) was significantly larger than in the soma ($\Delta F/F$: 10.4 ± 3.2, $p < 0.001$) or proximal dendrites ($\Delta F/F$: 14.9 ± 2.6; $p < 0.001$, $n = 6$, ANOVA followed by Newman–Keuls tests). Interestingly, the time course of I_{DHPG} most closely matches time course of $[Ca^{2+}]_i$ in the distal dendrite (Fig. 5*B*). In some cells, DHPG puffs that triggered a rise in $[Ca^{2+}]_i$ in the dendrites failed to alter $[Ca^{2+}]_i$ in the soma (Fig. 4*A*,*B*). Together, these results suggest that the intracellular stores triggering the rise in $[Ca^{2+}]_i$ and I_{DHPG} are located predominantly in ET cell dendrites.

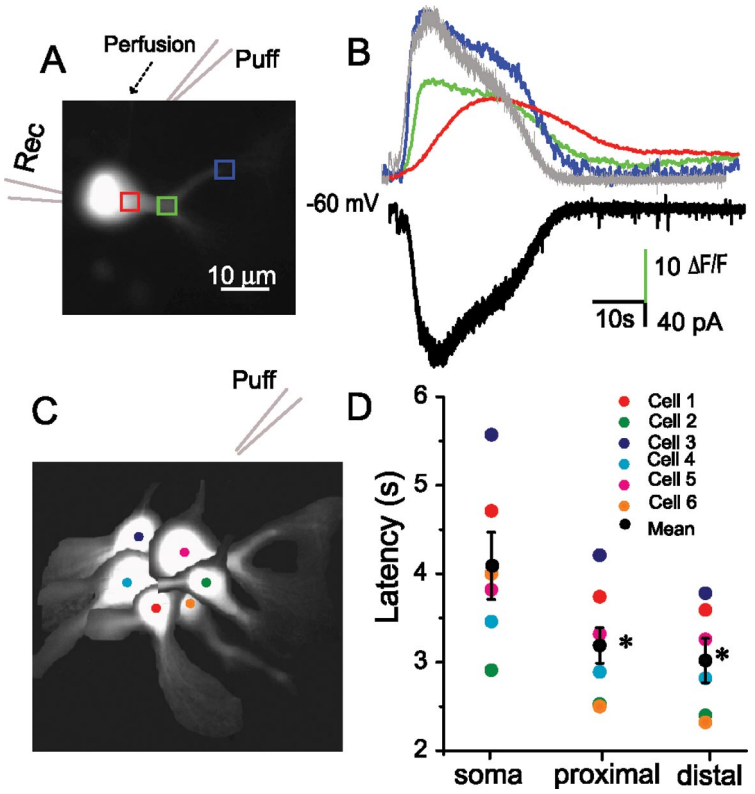

Figure 5. DHPG-evoked $[Ca^{2+}]_i$ transients originate in ET cell dendrites. ***A***, Fluorescence image of an ET cell recorded with a pipette containing 100 μM fura-2 and voltage clamped at −60 mV. ***B***, Time course of changes in $[Ca^{2+}]_i$ in the soma (red trace), proximal (green trace) and distal (blue trace) dendritic regions (corresponding to the rectangles in ***A1***), and inward current (black trace) elicited by a focal puff of DHPG (1 mM) 30 μm upstream from the soma; note that the time course of the inward current (inverted trace shown in gray) closely corresponds to that of the Ca^{2+} transient in the distal dendrite. Experiment was in conducted in normal ACSF (no antagonists). ***C***, Schematic diagram showing the position of six sampled ET cells with respect to the puffer pipette. ***D***, Individual cell and group data (mean ± SEM, black circles) showing that the latencies of $[Ca^{2+}]_i$ transients in the soma were longer than those in the dendrites (*$p < 0.001$, $n = 6$).

I_{CAN} antagonists suppressed I_{DHPG} and rhythmic bursting

mGluR-activated and other I_{CAN}s in a variety of neurons are attenuated by antagonists such as SKF96365 and FFA (Partridge and Valenzuela, 2000; Kim et al., 2003; Tozzi et al., 2003; Pressler and Strowbridge, 2006; Berg et al., 2007; Wang et al., 2007). Therefore, we investigated the effects of SKF96365 and FFA on I_{DHPG} in ET cells. Responses to DHPG (30 μM) were measured before and during bath application of SKF96365 (100 μM) or FFA (100 μM). As shown in Figure 6, *A* and *B*, SKF96365 and FFA produced similar effects, largely eliminating I_{DHPG} across the entire range of membrane poten-

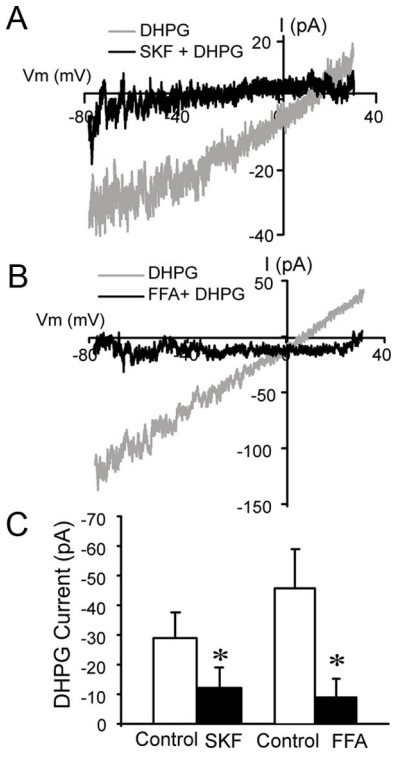

Figure 6. I_{DHPG} is attenuated by I_{CAN} antagonists. ***A***, ***B***, Subtraction *I–V* curves showing responses to DHPG (30 μM) before and during application of 100 μM SKF96365 (SKF, ***A***) or 100 μM FFA (***B***); data from different ET cells are shown in ***A*** and ***B***. ***C***, Group data show the magnitude of I_{DHPG} (HP = −60 mV) before (control) and during SKF ($n = 6$) or FFA ($n = 4$) application (*$p < 0.05$, paired *t* tests).

tials tested. SKF96365 and FFA significantly reduced the magnitude of I_{DHPG} measured at −60 mV by 50 ± 9.7% ($n = 6$) and 86.2 ± 12.6% ($n = 4$), respectively [$p < 0.05$ compared with control (DHPG alone), paired *t* tests] (Fig. 6*C*). As observed elsewhere, the effects of SKF96365 and FFA were poorly reversible within the time course of the recordings (Tozzi et al., 2003; Pace et al., 2007).

We next investigated whether the DHPG-evoked enhancement of rhythmic bursting in ET cells could be prevented by application of SKF96365 (100 μM). In current-clamp recordings (Fig. 7) (with CNQX-APV-gabazine in the bath), DHPG (30 μM) significantly enhanced rhythmic bursting as described earlier (Fig. 1). As shown in Figure 7, SKF96365 (100 μM) applied alone decreased the number of spikes per burst (2.7 ± 0.4 vs 2.2 ± 0.2), and the firing frequency (3.1 ± 1.2 Hz vs 0.6 ± 0.6 Hz; $n = 6$, $p < 0.05$, one-way repeated-measures ANOVA followed by Newman–Keuls tests). DHPG (30 μM) enhancement of bursting was diminished but not eliminated when applied in the presence of SKF96365. Statistically, the firing frequency, burst frequency, and number of spikes per burst evoked by DHPG were significantly reduced by SKF96365 ($n = 6$, $p < 0.05$ for each, one-way repeated-measures ANOVA followed by Newman–Keuls tests), but the burst duration was not significantly influenced (Fig. 7). These results suggest that DHPG-evoked enhancement of rhythmic bursting is in part due to I_{CAN}. The residual effects of DHPG on bursting in the presence of SKF96365 may be due to modulation of other currents in ET cells (see Discussion).

DHPG induces slow rhythmic oscillations in ET cells

Activation of mGluRs generates synchronous membrane potential oscillations in electrically coupled brainstem, thalamic, and cortical neurons when ionotropic glutamate and GABA receptors are blocked (Beierlein et al., 2000; Hughes et al., 2002a,b, 2004; Sharifullina et al., 2005). ET cells of the same glomerulus are coupled by electrical synapses that generate slow membrane current oscillations and spikelets in these cells (Hayar et al., 2005). We reasoned, therefore, that DHPG-evoked increases in the strength of ET cell spike bursts should enhance the frequency and/or amplitude of oscillations and spikelets. We measured spontaneous membrane currents in ET cells (HP = −60 mV) using internal solution containing CsCl to block intrinsic voltage-gated K^+ channels and QX-314 (10 mM) to block Na^+ channels with APV-CNQX-gabazine in the bath. Under these conditions, spontaneous membrane current oscillations were observed at a relatively low frequency of 0.4 ± 0.1 Hz (Fig. 8*A*). Smaller amplitude, faster spikelets were typically superimposed on these oscillations with a mean of 2.5 ± 0.4 spikelets per oscillation (Fig. 8*A*,*B*). Compared with baseline, DHPG (3, 10, and 30 μM; $n = 7$) significantly increased the frequency of the oscillations to 1.3 ± 0.1 Hz, 1.8 ± 0.1 Hz, and 2.1 ± 0.2 Hz, respectively ($p < 0.001$ for each, one-way repeated-measures ANOVA followed by Newman–Keuls tests) (Fig. 8*A*). DHPG also increased the regularity of the oscillations, as evident by the enhanced sideband in membrane current autocorrelograms (Fig. 8*C*). The coefficient of autocorrelation (measured as the peak of the first sideband in the autocorrelogram) increased in 5 of 7 ET cells, from 0.2 ± 0.1 to 0.5 ± 0.2 (10 μM DHPG, $p < 0.01$, paired *t* test). DHPG (3, 10, and 30 μM; $n = 7$) increased the number of spikelets per oscillation to 5.8 ± 0.6, 7.5 ± 0.7, and 10.1 ± 0.7, respectively ($p < 0.001$ for each compared with baseline, one-way repeated-measures ANOVA followed by Newman–Keuls tests) (Fig. 8*B*). Similar results were observed when VGCCs were blocked by extracellular application of Cd (100 μM) and Ni (1 mM); the oscillation frequency (1.9 ± 0.1 Hz) and the number of spikelets per oscillation (14.5 ± 1.3 Hz) with 30 μM DHPG did not differ from values in the absence of Cd and Ni ($p > 0.05$, $n = 5$ unpaired *t* tests, data not shown). In contrast, bath-applied DHPG (30 μM) did not induce oscillations or spikelets in the presence of TTX-APV-CNQX-gabazine ($n = 35$). Together, these findings suggest that the DHPG-evoked oscillations and spikelets are generated by electrotonic network interactions that do not involve VGCCs or Ca^{2+}-dependent synaptic transmission.

Discussion

Our results demonstrate that activation of group I mGluRs increases the strength of rhythmic bursting and induces slow membrane current oscillations in ET cells. The increase in bursting strength is due, at least in part, to activation of an I_{CAN} triggered in ET cell dendrites secondarily to a rise in intracellular Ca^{2+} derived from intracellular stores. The slow oscillations elicited by DHPG appear to be a network phenomenon involving spike burst-driven electrotonic interactions among ET cells. Intraglomerular activity is synchronized by ET cells and olfactory input elicits slow mGluR-dependent rhythmic oscillations that are synchronous among mitral cells of the same glomerulus. We hypothesize that mGluRs play a critical role in slow respiratory-driven activity by enhancing output of an intrinsically rhythmic neuronal element of the MOB, ET cells, which in turn synchronize the intraglomerular network oscillations via electrical and chemical synapses.

mGluR1/5 enhance ET cell excitability via I_{CAN} activation

DHPG increased ET cell excitability by engaging an I_{CAN} current linked to mGluR1/5 as observed previously (Gee et al., 2003). I_{DHPG} in ET cells appears to be activated secondarily to Ca^{2+} release from intracellular stores, and was characterized by increased membrane conductance, a reversal potential near 0 mV, and Na^+ as the major inward charge carrier; K^+ and Ca^{2+} permeability of the I_{CAN} channels requires additional study. DHPG produced a rapid rise in dendritic $[Ca^{2+}]_i$ that paralleled I_{DHPG}. The distal dendritic Ca^{2+} transients preceded those in the soma and I_{CAN} currents returned to baseline while somatic $[Ca^{2+}]_i$ was still elevated, indicating that channels mediating the current are located primarily in ET cell dendrites. However, the contribution of somatic I_{CAN} may have been underestimated in the present study if somatic $[Ca^{2+}]_i$ transients were insufficient to activate somatic I_{CAN} channels or if somatic I_{CAN} is small relative to the dendrites.

I_{DHPG} was attenuated by SKF96365 and FFA, which are known to block I_{CAN} and transient receptor potential (TRP) channel-mediated cationic currents in a variety of neurons (Gee et al., 2003; Kim et al., 2003; Tozzi et al., 2003; Bengtson et al., 2004; Schiller, 2004; Zhu et al., 2004, 2005; Pressler and Strowbridge, 2006; Ramsey et al., 2006; Berg et al., 2007; Pace et al., 2007; Pressler et al., 2007; Wang et al., 2007). Unidentified glomerular layer neurons express several TRP channel subtypes, including TRPC4/5 (Philipp et al., 1998), raising the possibility that I_{DHPG} in ET cells may correspond to a TRPC channel. Results with FFA and SKF96365 should be interpreted with some caution, however, as these agents are known to modulate other voltage-dependent currents and intracellular Ca^{2+} mobilization (Merritt et al., 1990; Ottolia and Toro, 1994; Greenwood et al., 1995; Kochetkov et al., 2000; Ghamari-Langroudi and Bourque, 2002; Pressler and Strowbridge, 2006).

mGluR1/5 activation increases the strength of ET cell rhythmic bursting

The reversal potential of I_{DHPG} is more positive than the ET cell resting membrane potential, hence DHPG would be expected to depolarize and increase ET cell excitability. Consistent with this, DHPG moderately depolarized ET cells, and increased the bursting frequency and the number of spikes per burst. Previous studies indicate that steady current injec-

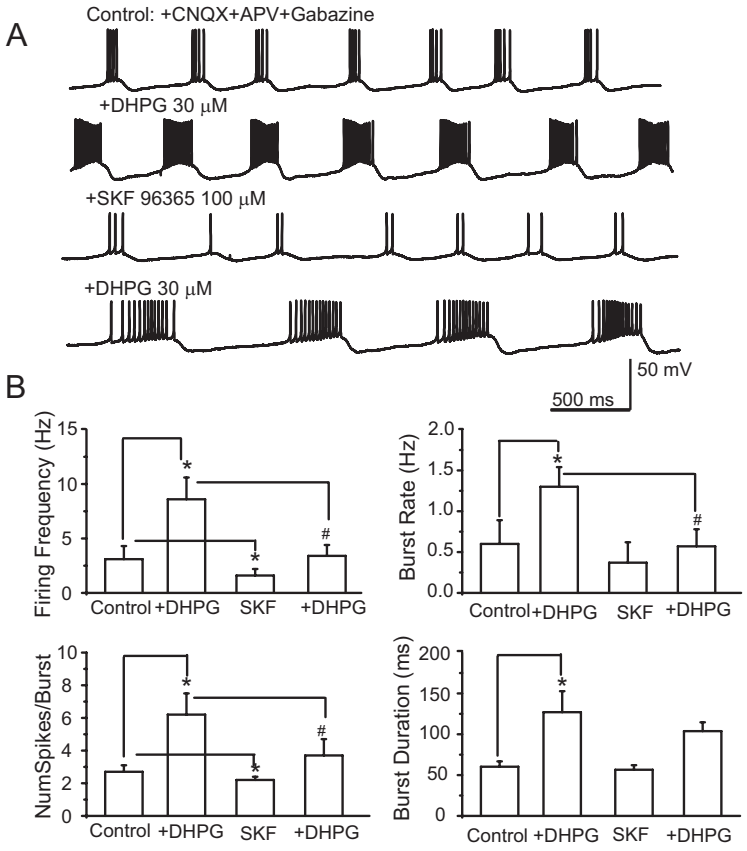

Figure 7. I_{CAN} antagonists dampen ET cell rhythmic bursting. ***A***, Current-clamp recordings showing that ET cell bursting is enhanced by DHPG (30 μM). After DHPG washout, SKF96365 (100 μM) dampened basal and DHPG-evoked bursting; experiment performed in the presence of CNQX-APV-gabazine (control). ***B***, Group data summarizing the effects of DHPG and SKF on properties of ET cell bursting. $n = 6$, $^*p < 0.05$ versus control, $^\#p < 0.05$ DHPG versus DHPG + SKF; one-way repeated-measures ANOVA followed by Newman–Keuls tests.

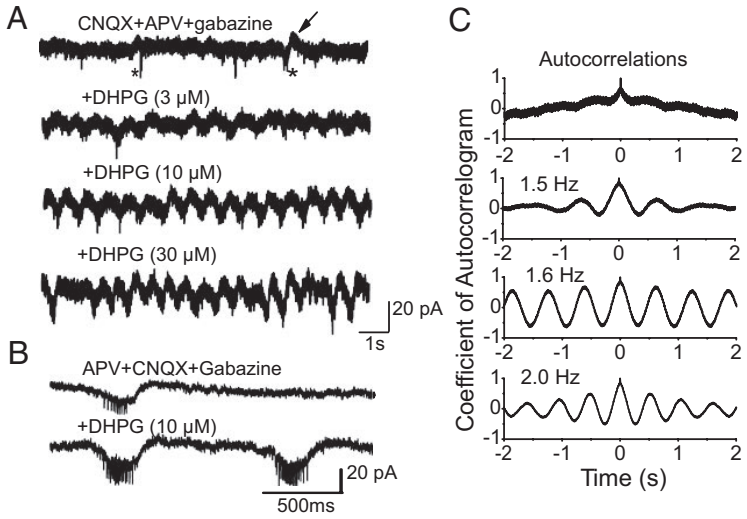

Figure 8. DHPG induces slow rhythmic oscillations in ET cells. ***A***, Recordings from an ET cell were made in voltage-clamp mode (HP = −60 mV) using a pipette containing CsCl and QX-314 in the presence of CNQX + APV + gabazine. Top trace, Under these recording conditions, small infrequent slow membrane current oscillations (arrow) and spikelets (asterisks) occurred. Bottom three traces, DHPG dose-dependently increased the oscillation frequency from <1 Hz (control) before to 2.0 Hz (30 μM DHPG). Note also that DHPG increased the amplitude of slow oscillations in a concentration-dependent manner. ***B***, Faster time scale records showing oscillations and spikelets before and during DHPG application. ***C***, Autocorrelograms of membrane current oscillations corresponding to the four conditions shown in ***A***. Note that DHPG increased the regularity of the oscillations as shown by an enhanced sideband in the autocorrelograms.

tion into ET cells producing depolarization comparable to that evoked by DHPG increases the burst frequency but decreases the number of spikes per burst (Hayar et al., 2004a). Thus, direct ET depolarization mimics the increase in burst frequency but not the increase in spikes per burst produced by DHPG. This indicates DHPG, in addition to I_{CAN}, modulates one or more of the several inward and outward intrinsic conductances that cooperatively regulate ET cell spike bursts (Liu and Shipley, 2008). Consistent with this possibility, SKF96365, which largely eliminated the I_{CAN}, significantly reduced but did not completely antagonize DHPG-evoked enhancement of bursting. DHPG may also facilitate persistent Na^+ (I_{NaP}) or voltage-activated Ca^{2+} currents underlying ET cell bursting (Hayar et al., 2004a; Liu and Shipley, 2008). Indeed, preliminary studies indicate that DHPG enhances I_{NaP} in ET cells (Dong et al., 2007). DHPG may also negatively modulate the large-conductance Ca^{2+}-dependent K^+ current (I_{BK}) that limits the burst duration and the number of spikes per burst (Liu and Shipley, 2008). ET cell bursting may also be enhanced by gap junction-mediated interactions among electrically coupled ET cells (Hayar et al., 2005).

Functional impact on the glomerular network

ET cells play important roles in coordinating intraglomerular network activity. ET cells within the same glomerulus exhibit synchronous activity and synchronize the activity of mitral cells and GABAergic periglomerular cells (Hayar et al., 2004b, 2005; Murphy et al., 2005; De Saint Jan et al., 2009). GABA release from periglomerular cells is enhanced by sustained depolarization via activation of NMDA receptors and high-voltage-activated Ca^{2+} currents (Hayar et al., 2005; Murphy et al., 2005). The mGluR-evoked enhancement of burst strength would increase presynaptic glutamate release from ET dendrites, amplifying periglomerular cell depolarization, GABA release, and intraglomerular inhibition (Hayar et al., 2005). mGluR-driven intracellular Ca^{2+} release may play an additional functional role in dendrodendritic inhibition in the glomeruli by facilitating glutamate release from ET cell dendrites.

Group I mGluR activation is necessary for slow rhythmic oscillatory activity within the glomeruli. mGluR1 blockade attenuates olfactory nerve-evoked 2 Hz oscillatory activity that is synchronous among mitral cells of the same glomerulus (Schoppa and Westbrook, 2001; De Saint Jan and Westbrook, 2005; Christie and Westbrook, 2006). Similar olfactory nerve-evoked mGluR1-mediated slow oscillations occur in mitral cell dendrites when ionotropic glutamate receptors and intrinsic Na^+ channels are blocked (Yuan and Knopfel, 2006). Such synchronized oscillations are thought to involve an interplay of electrical synapses and regenerative glutamate release from mitral/tufted cell dendrites within the glomerulus (Schoppa and Westbrook, 2001; De Saint Jan and Westbrook, 2005; Christie and Westbrook, 2006).

Our findings show that DHPG induced slow, 1.5–2.0 Hz membrane current oscillations and spikelets in ET cells when intrinsic K^+ and Na^+ channels were blocked, and when chemical transmission was eliminated by ionotropic glutamate/GABA receptor and VGCC antagonists. In contrast, DHPG-evoked oscillations and spikelets were not observed in the presence of TTX, suggesting that they arise via spike-driven network activity. In the absence of chemical synapses, ET cells of the same glomerulus communicate mainly via gap junctions that synchronize spontaneous membrane current oscillations and spikelets among these cells (Hayar et al., 2005). Accordingly, we hypothesize that DHPG-evoked oscillations are in large part a network-driven, electrical synapse-dependent phenomenon mediated by an increase in the strength, and perhaps synchrony, of bursts across the glomerular ensemble of ET cells. Consistent with this hypothesis, the DHPG-evoked increase in the number of spikes per burst is paralleled by a corresponding increase in the number of spikelets per oscillation, and the enhanced regularity of oscillations observed is indicative of increased synchrony among ET cells. The basal oscillation frequency (0.4 Hz) is lower than the mean bursting frequency of ET cells. The oscillations, however, were measured in conditions (APV-CNQX-gabazine, intracellular QX-314) that dampen ET cell excitability and membrane currents (e.g., I_{NaP}) that would otherwise amplify oscillatory activity. For example, ionotropic glutamate receptor blockade reduces ET cell burst strength (but not frequency) and would therefore dampen chemical and electrical transmission among ET cells (Hayar et al., 2004a, 2005; Hayar and Ennis, 2007). Additionally, synchronous bursts among coupled ET cells occur at a lower frequency than the intrinsic burst frequency of either cell (Hayar et al., 2004b, 2005). Thus, if oscillations are mediated by burst-driven interactions among ET cells as hypothesized, then the basal frequency of the oscillations in our experimental conditions would be expected to be lower than the mean bursting frequency of ET cells.

ET cell gap junctions have a relatively low conductance (0.1 nS) (Hayar et al., 2005) and may operate primarily as low-pass filters as in the retina, thalamic reticular nucleus, and substantia nigra (Landisman et al., 2002; Veruki and Hartveit, 2002; Vandecasteele et al., 2005). An important functional role of gap junctions in ET cells dendrites may be to filter fast spiking activity and propagate slow membrane potential oscillations. Based on these considerations, it is reasonable to speculate that ET cells play a particularly important role in spontaneous or olfactory nerve-evoked, mGluR-dependent slow oscillations in mitral cells. The frequency of DHPG-evoked oscillations corresponds well to those evoked by olfactory nerve stimulation and to the 1.5–2.0 Hz spontaneous burst frequency exhibited by the majority of ET cells in slices (Hayar et al., 2004a, 2005). ET cells were recently shown to drive synchronized spontaneous slow depolarizations among mitral cells via electrical and chemical synapses (De Saint Jan et al., 2009). Additionally, ET cells were found to amplify weak olfactory nerve input to mitral cells. Together with these results, our findings are consistent with growing evidence that ET cells play a key role in generating rhythmic oscillatory activity that synchronizes glomerular activity to olfactory input, which is itself tuned to sniffing of the animal (Hayar et al., 2004a,b, 2005; Wachowiak and Shipley, 2006; De Saint Jan et al., 2009).

References

Anwyl R (1999) Metabotropic glutamate receptors: electrophysiological properties and role in plasticity. Brain Res Rev 29:83–120.

Beierlein M, Gibson JR, Connors BW (2000) A network of electrically coupled interneurons drives synchronized inhibition in neocortex. Nat Neurosci 3:904–910.

Bengtson CP, Tozzi A, Bernardi G, Mercuri NB (2004) Transient receptor potential-like channels mediated metabotropic glutamate receptor EPSCs in rat dopamine neurones. J Physiol 555:323–330.

Berg AP, Sen N, Bayliss DA (2007) TrpC3/C7 and slo2.1 are molecular targets for metabotropic glutamate receptor signaling in rat striatal cholinergic interneurons. J Neurosci 27:8845–8856.

Buonviso N, Amat C, Litaudon P (2006) Respiratory modulation of olfactory neurons in the rodent brain. Chem Senses 31:145–154.

Carlson GC, Slawecki ML, Lancaster E, Keller A (1997) Distribution and activation of intracellular Ca2+ stores in cultured olfactory bulb neurons. J Neurophysiol 78:2176–2185.

Christie JM, Westbrook GL (2006) Lateral excitation within the olfactory bulb. J Neurosci 26:2269–2277.

Crépel V, Aniksztejn L, Ben-Ari Y, Hammond C (1994) Glutamate metabotropic receptors increase a Ca (2+)-activated nonspecific cationic current in CA1 hippocampal neurons. J Neurophysiol 72:1561–1569.

De Saint Jan D, Westbrook GL (2005) Detecting activity in olfactory bulb glomeruli with astrocyte recording. J Neurosci 25:2917–2924.

De Saint Jan D, Westbrook GL (2007) Disynaptic amplification of metabotropic glutamate receptor 1 responses in the olfactory bulb. J Neurosci 27:132–140.

De Saint Jan D, Hirnet D, Westbrook GL, Charpak S (2009) External tufted cells drive the output of the olfactory bulb glomeruli. J Neurosci 29:2043–2052.

Dong HW, Hayar A, Ennis M (2007) Activation of group I mGluRs enhances rhythmic bursting and nonselective cation currents in olfactory bulb external tufted cells. Soc Neurosci Abstr 33:277.2.

Ennis M, Zhu M, Heinbockel T, Hayar A (2006) Olfactory nerve-evoked, metabotropic glutamate receptor-mediated synaptic responses in rat olfactory bulb mitral cells. J Neurophysiol 95:2233–2241.

Finch EA, Augustine GJ (1998) Local calcium signalling by inositol-1,4,5-trisphosphate in Purkinje cell dendrites. Nature 396:753–756.

Fontanini A, Bower JM (2006) Slow-waves in the olfactory system: an olfactory perspective on cortical rhythms. Trends Neurosci 29:429–437.

Fotuhi M, Sharp AH, Glatt CE, Hwang PM, von Krosigk M, Snyder SH, Dawson TM (1993) Differential localization of phosphoinositide-linked metabotropic glutamate receptor (mGluR1) and the inositol 1,4,5-triphosphate receptor in rat brain. J Neurosci 13:2001–2012.

Gee CE, Benquet P, Gerber U (2003) Group I metabotropic glutamate receptors activate a calcium-sensitive transient receptor potential-like conductance in rat hippocampus. J Physiol 546:655–664.

Ghamari-Langroudi M, Bourque CW (2002) Flufenamic acid blocks depolarizing afterpotentials and phasic firing in rat supraoptic neurones. J Physiol 545: 537–542.

Greenwood IA, Hogg RC, Large WA (1995) Effect of frusemide, ethacrynic acid and indanyloxyacetic acid on spontaneous Ca-activated currents in rabbit portal vein smooth muscle cells. Br J Pharmacol 115:733–738.

Hayar A, Ennis M (2007) Endogenous GABA and glutamate finely tune the bursting of olfactory bulb external tufted cells. J Neurophysiol 98:1052–1056.

Hayar A, Karnup S, Shipley MT, Ennis M (2004a) Olfactory bulb glomeruli: external tufted cells intrinsically burst at theta frequency and are entrained by patterned olfactory input. J Neurosci 24:1190–1199.

Hayar A, Karnup S, Ennis M, Shipley MT (2004b) External tufted cells: a major excitatory element that coordinates glomerular activity. J Neurosci 24:6676–6685.

Hayar A, Shipley MT, Ennis M (2005) Olfactory bulb external tufted cells are synchronized by multiple intraglomerular mechanisms. J Neurosci 25:8197–8208.

Heinbockel T, Heyward P, Conquet F, Ennis M (2004) Regulation of main olfactory bulb mitral cell excitability by metabotropic glutamate receptor mGluR1. J Neurophysiol 92:3085–3096.

Hughes SW, Blethyn KL, Cope DW, Crunelli V (2002a) Properties and origin of spikelets in thalamocortical neurones in vitro. Neuroscience 110:395–401.

Hughes SW, Cope DW, Blethyn KL, Crunelli V (2002b) Cellular mechanisms of the slow (<1 Hz) oscillation in thalamocortical neurons in vitro. Neuron 33:947–958.

Hughes SW, Lörincz M, Cope DW, Blethyn KL, Kékesi KA, Parri HR, Juhász G, Crunelli V (2004) Synchronized oscillations at alpha and theta frequencies in the lateral geniculate nucleus. Neuron 42:253–268.

Keele NB, Arvanov VL, Shinnick-Gallagher P (1997) Quisqualate-preferring metabotropic glutamate receptor activates Na (+)-Ca2+ exchange in rat basolateral amygdala neurones. J Physiol 499:87–104.

Kim J, Chung YD, Park DY, Choi S, Shin DW, Soh H, Lee HW, Son W, Yim J, Park CS, Kernan MJ, Kim C (2003) A TRPV family ion channel required for hearing in *Drosophila*. Nature 424:81–84.

Kochetkov KV, Kazachenko VN, Marinov BS (2000) Dose-dependent potentiation and inhibition of single Ca2+-activated K+ channels by flufenamic acid. Membr Cell Biol 14:285–298.

Landisman CE, Long MA, Beierlein M, Deans MR, Paul DL, Connors BW (2002) Electrical synapses in the thalamic reticular nucleus. J Neurosci 22:1002–1009.

Lasser-Ross N, Miyakawa H, Lev-Ram V, Young SR, Ross WN (1991) High time resolution fluorescence imaging with a CCD camera. J Neurosci Methods 36:253–261.

Lee K, Boden PR (1997) Characterization of the inward current induced by metabotropic glutamate receptor stimulation in rat ventromedial hypothalamic neurones. J Physiol 504: 649–663.

Liu S, Shipley MT (2008) Multiple conductances cooperatively regulate spontaneous bursting in mouse olfactory bulb external tufted cells. J Neurosci 28:1625–1639.

Llano I, Dreessen J, Kano M, Konnerth A (1991) Intradendritic release of calcium induced by glutamate in cerebellar Purkinje cells. Neuron 7:577–583.

Martin LJ, Blackstone CD, Huganir RL, Price DL (1992) Cellular localization of a metabotropic glutamate receptor in rat brain. Neuron 9:259–270.

Masu M, Tanabe Y, Tsuchida K, Shigemoto R, Nakanishi S (1991) Sequence and expression of a metabotropic glutamate receptor. Nature 349: 760–765.

Merritt JE, Armstrong WP, Benham CD, Hallam TJ, Jacob R, Jaxa-Chamiec A, Leigh BK, McCarthy SA, Moores KE, Rink TJ (1990) SK&F 96365, a novel inhibitor of receptor-mediated calcium entry. Biochem J 271: 515–522.

Murphy GJ, Darcy DP, Isaacson JS (2005) Intraglomerular inhibition: signaling mechanisms of an olfactory microcircuit. Nat Neurosci 8:354–364.

Ottolia M, Toro L (1994) Potentiation of large conductance KCa channels by niflumic, flufenamic, and mefenamic acids. Biophys J 67:2272–2279.

Pace RW, Mackay DD, Feldman JL, Del Negro CA (2007) Inspiratory bursts in the preBötzinger complex depend on a calcium-activated non-specific cation current linked to glutamate receptors in neonatal mice. J Physiol 582:113–125.

Partridge LD, Valenzuela CF (2000) Block of hippocampal CAN channels by flufenamate. Brain Res 867:143–148.

Philipp S, Hambrecht J, Braslavski L, Schroth G, Freichel M, Murakami M, Cavalié A, Flockerzi V (1998) A novel capacitative calcium entry channel expressed in excitable cells. EMBO J 17:4274–4282.

Pressler RT, Strowbridge BW (2006) Blanes cells mediate persistent feedforward inhibition onto granule cells in the olfactory bulb. Neuron 49:889–904.

Pressler RT, Inoue T, Strowbridge BW (2007) Muscarinic receptor activation modulates granule cell excitability and potentiates inhibition onto mitral cells in the rat olfactory bulb. J Neurosci 27:10969–10981.

Ramsey IS, Delling M, Clapham DE (2006) An introduction to TRP channels. Annu Rev Physiol 68:619–647.

Romano C, Sesma MA, McDonald CT, O'Malley K, Van den Pol AN, Olney JW (1995) Distribution of metabotropic glutamate receptor mGluR5 immunoreactivity in rat brain. J Comp Neurol 355:455–469.

Sagara Y, Fernandez-Belda F, de Meis L, Inesi G (1992) Characterization of the inhibition of intracellular Ca^{2+} transport ATPases by thapsigargin. J Biol Chem 267:12606–12613.

Sahara Y, Kubota T, Ichikawa M (2001) Cellular localization of metabotropic glutamate receptors mGluR1, 2/3, 5 and 7 in the main and accessory olfactory bulb of the rat. Neurosci Lett 312:59–62.

Schiller Y (2004) Activation of a calcium-activated cation current during epileptiform discharges and its possible role in sustaining seizure-like events in neocortical slices. J Neurophysiol 92:862–872.

Schoppa NE, Westbrook GL (2001) Glomerulus-specific synchronization of mitral cells in the olfactory bulb. Neuron 31:639–651.

Scott JW (2006) Sniffing and spatiotemporal coding in olfaction. Chem Senses 31:119–130.

Sharifullina E, Ostroumov K, Nistri A (2005) Metabotropic glutamate receptor activity induces a novel oscillatory pattern in neonatal rat hypoglossal motoneurones. J Physiol 563:139–159.

Shigemoto R, Nakanishi S, Mizuno N (1992) Distribution of the mRNA for a metabotropic glutamate receptor (mGluR1) in the central nervous system: an in situ hybridization study in adult and developing rat. J Comp Neurol 322:121–135.

Staub C, Vranesic I, Knöpfel T (1992) Responses to metabotropic glutamate receptor activation in cerebellar Purkinje cells: induction of an inward current. Eur J Neurosci 4:832–839.

Takechi H, Eilers J, Konnerth A (1998) A new class of synaptic response involving calcium release in dendritic spines. Nature 396:757–760.

Tempia F, Alojado ME, Strata P, Knöpfel T (2001) Characterization of the

mGluR (1)-mediated electrical and calcium signaling in Purkinje cells of mouse cerebellar slices. J Neurophysiol 86:1389–1397.

Tozzi A, Bengtson CP, Longone P, Carignani C, Fusco FR, Bernardi G, Mercuri NB (2003) Involvement of transient receptor potential-like channels in responses to mGluR-I activation in midbrain dopamine neurons. Eur J Neurosci 18:2133–2145.

Vandecasteele M, Glowinski J, Venance L (2005) Electrical synapses between dopaminergic neurons of the substantia nigra pars compacta. J Neurosci 25:291–298.

van den Pol AN (1995) Presynaptic metabotropic glutamate receptors in adult and developing neurons: autoexcitation in the olfactory bulb. J Comp Neurol 359:253–271.

Veruki ML, Hartveit E (2002) Electrical synapses mediate signal transmission in the rod pathway of the mammalian retina. J Neurosci 22:10558–10566.

Wachowiak M, Shipley MT (2006) Coding and synaptic processing of sensory information in the glomerular layer of the olfactory bulb. Semin Cell Dev Biol 17:411–423.

Wang M, Bianchi R, Chuang SC, Zhao W, Wong RK (2007) Group I metabotropic glutamate receptor-dependent TRPC channel trafficking in hippocampal neurons. J Neurochem 101:411–421.

Yuan Q, Knöpfel T (2006) Olfactory nerve stimulation-evoked mGlur1 slow potentials, oscillations and calcium signaling in mouse olfactory bulb mitral cells. J Neurophysiol 95:3097–3104.

Yuzaki M, Mikoshiba K (1992) Pharmacological and immunocytochemical characterization of metabotropic glutamate receptors in cultured Purkinje cells. J Neurosci 12:4253–4263.

Zhu ZT, Munhall A, Shen KZ, Johnson SW (2004) Calcium-dependent subthreshold oscillations determine bursting activity induced by N-methyl-D-aspartate in rat subthalamic neurons in vitro. Eur J Neurosci 19:1296–1304.

Zhu ZT, Munhall A, Shen KZ, Johnson SW (2005) NMDA enhances a depolarization-activated inward current in subthalamic neurons. Neuropharmacology 49:317–327.